Dynamics of two vibro-impact nonlinear energy sinks in parallel under periodic and transient excitations

Tao Li, Etienne Gourc, Sébastien Seguy, Alain Berlioz

Dynamics of two vibro-impact nonlinear energy sinks in parallel under periodic and transient excitations

T. Li[a], E. Gourc[b], S. Seguy[a], A. Berlioz[a]

[a] *Université de Toulouse, Institut Clément Ader (ICA), CNRS-INSA-ISAE-Mines Albi-UPS,Toulouse, France*

[b] *Space Structures and Systems Laboratory, Department of Aerospace and Mechanical Engineering, University of Liege, 1 Chemin des Chevreuils (B52/3), B-4000 Liege, Belgium*

Abstract

A linear oscillator (LO) coupled with two vibro-impact (VI) nonlinear energy sinks (NES) in parallel is studied under periodic and transient excitations, respectively. The objective is to study response regimes and to compare their efficiency of vibration control. Through the analytical study with multiple scales method, two slow invariant manifolds (SIM) are obtained for two VI NES, and different SIM that result from different clearances analytically supports the principle of separate activation. In addition, fixed points are calculated and their positions are applied to judge response regimes. Transient responses and modulated responses can be further explained. By this way, all analysis is around the most efficient response regime. Then, numerical results demonstrate two typical responses and validate the effectiveness of analytical prediction. Finally, basic response regimes are experimentally observed and analyzed, and they can well explain the complicated variation of responses and their corresponding efficiency, not only for periodic excitations with a fixed frequency or a range of frequency, but also for transient excitation. Generally, vibration control is more effective when VI NES is activated with two impacts per cycle, whatever the types of excitation and the

Email address: tli@insa-toulouse.fr (T. Li)

combinations of clearances. This observation is also well reflected by the separate activation of two VI NES with two different clearances, but at different levels of displacement amplitude of LO.

Keywords: Vibro-impact, Targeted energy transfer, Nonlinear energy sink, Impact damper

1. Introduction

The excessive vibration energy of a targeted system can be dissipated by using an auxiliary device, which absorbs and dissipates such undesired energy by producing a force opposing it, either continuously such as in the case of nonlinear energy sink (NES) with continuous nonlinearity [1, 2, 3, 4, 5] or segmentally by NES with piece-wise nonlinearity [6] or intermittently and instantly by impact damper [7]. Due to its simplicity of construction, fast response at the initial stage of perturbation and effectiveness at a broadband frequency, impact damper has been studied several decades ago [8, 9], no matter the case with only one impact pair [10, 11, 12, 13, 14] or multi-units with several impact-pairs [15, 16, 17, 18, 19, 20].

Recently, impact damper is studied further and more clear under the context of targeted energy transfer (TET) [21, 22] and termed as vibro-impact (VI) NES [23, 24, 25]. Its mechanism of TET is revealed by studying its Hamiltonian system [26], and it is observed that some special orbits are responsible for the irreversible transfer of energy from a main system to an attached VI NES. Through directly studying the system with damping, a slow invariant manifold (SIM), which is firstly used for the analysis of a NES with cubic nonlinearity [27, 28], can be obtained by multiple scales method and be applied to analyze response regimes [29, 30, 31, 32, 33]. As a result, transient responses and unsteady responses such

as chaotic strongly modulated response (SMR) can be well explained for the first time [31, 34]. Dynamics, such as response regimes and bifurcations, is comprehensively re-analyzed around SIM [35], more specifically, around the regime with two impacts per cycle. In [36], the efficiency of different response regimes around SIM is compared, and the response regime with two impact per cycle and around the entrance of SMR is found to be optimal. Based on this efficiency comparison of response regimes, a common optimization design criterion of VI NES is proposed for different excitation types, and the central idea is to make the most efficient response regime with two impacts per cycle exist or last as long as possible. Therefore, it is natural to expect the following design criterion for multi VI NES: to make each VI NES activated with this optimal response regime.

About its application, any analytical study of nonlinear systems coupled with NES will be difficult, no matter this nonlinear system is a turning system [37] or a helicopter system [38], or even a simple rod [39]. For VI NES, a solution is to found its activation condition without considering the specific type of a targeted system. It is found that the activation of a VI NES is limited to a range of displacement amplitude of a linear system [36]. From the viewpoint of energy, it means that its effectiveness is not only limited by a minimal value (activation threshold) but also a maximal value. Therefore, it is natural to increase the range of effectiveness of vibration control by designing different VI NES with different activation ranges for both linear and nonlinear systems. In this way, the efficiency and robustness of TET can be improved, even at small energy levels.

About multi NES, there already exist extensive studies [40, 41, 42, 43], and normally frequency components are used as indices to judge the possible transient or sustained resonance captures, and to identify different levels of activation.

However, this kind of index will not be used here for VI NES, since the impact number per cycle is a more direct measure. For example, the response regime with two impacts per cycle can be easily distinguished from numerical or experimental viewpoints, and actually it corresponds to 1:1 resonance. Although frequency components can be calculated by wavelet transform, it will not make the analysis easier and will not be used here.

In addition to the viewpoint of TET, the analytical study of systems coupled with multi VI NES also deserves further investigation fortwo reasons. Firstly, the research of multi VI NES is closely related to particle dampers [44]. Secondly, complicated response regimes such as intermittent beating responses [18, 19] need further analytical explanations rather than only analytical treatments of steady periodic regimes [16, 20].

Therefore, the objective of this paper is to generalize the optimization design criterion for one VI NES [36] to multiple VI NES. The focus is still around response regimes, efficiency and the relation between them. The impact number per cycle is used to characterize response regimes and corresponding TET.

The paper is organized as follows: a linear oscillator (LO) coupled with two VI NES in parallel under periodic excitation is analytically developed in Section 2. Then, numerical validations are demonstrated. In Section 4, experimental results under periodic and transient excitations are demonstrated for different conditions. Finally, a conclusion is addressed.

2. Analytical development

The considered system is presented in Fig. 1. Two VI NES in parallel are attached to a LO. The equation of motion between impacts is expressed as follows:

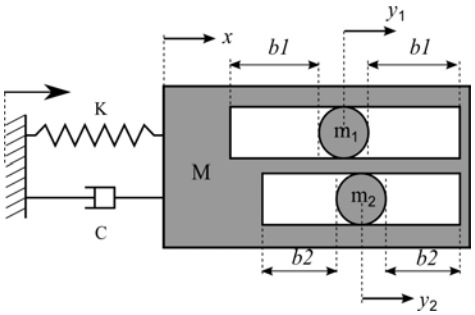

Fig. 1. Schema of a LO with two VI NES coupled in parallel.

$$
\begin{aligned}
&M\frac{d^2x}{dt^2}+C\frac{dx}{dt}+Kx=F\sin\Omega t\\
&m_1\frac{d^2y_1}{dt^2}=0, \quad \forall|x-y_1|<b1\\
&m_2\frac{d^2y_2}{dt^2}=0, \quad \forall|x-y_2|<b2
\end{aligned}
\tag{1}
$$

The motion relation between states before and after impacts can be obtained under the condition of simplified impact theory and conservation of momentum and it can be written as:

$$
\begin{aligned}
&\forall|x-y_1|=b1 \quad \text{or } |x-y_2|=b2\\
&x_+=x_-, \quad y_{1+}=y_{1-}, \quad y_{2+}=y_{2-}\\
&M\frac{dx_+}{dt}+m_1\frac{dy_{1+}}{dt}+m_2\frac{dy_{2+}}{dt}=M\frac{dx_-}{dt}+m_1\frac{dy_{1-}}{dt}+m_2\frac{dy_{2-}}{dt}\\
&\text{if } |x-y_1|=b1\\
&\frac{dx_+}{dt}-\frac{dy_{1+}}{dt}=-R\left(\frac{dx_-}{dt}-\frac{dy_{1-}}{dt}\right), \quad \frac{dy_{2+}}{dt}=\frac{dy_{2-}}{dt}\\
&\text{if } |x-y_2|=b2\\
&\frac{dx_+}{dt}-\frac{dy_{2+}}{dt}=-R\left(\frac{dx_-}{dt}-\frac{dy_{2-}}{dt}\right), \quad \frac{dy_{1+}}{dt}=\frac{dy_{1-}}{dt}
\end{aligned}
\tag{2}
$$

The subscripts $+$ and $-$ indicate time immediately after and before impacts.

R represents the restitution coefficient of impact. The dimensionless variables as follows are introduced:

$$\begin{aligned}
&\omega^2 = \frac{K}{M}, \quad T = \omega t, \quad \lambda = \frac{C}{(m_1+m_2)\omega}, \quad \varepsilon = \frac{m_1+m_2}{M},\\
&G = \frac{F}{(m_1+m_2)\omega^2}, \quad X = \frac{x}{b1}, \quad Y_1 = \frac{y_1}{b1},\\
&Y_2 = \frac{y_2}{b1}, \quad \Delta = \frac{b2}{b1}, \quad \alpha_i = \frac{m_i}{m_1+m_2}, \quad \tilde{\Omega} = \frac{\Omega}{\omega}
\end{aligned} \tag{3}$$

After substitution of Eq.(3) in Eq.(1), it becomes:

$$\begin{aligned}
&\ddot{x} + \varepsilon\lambda\dot{X} + X = \varepsilon G \sin\tilde{\Omega}T,\\
&\varepsilon\alpha_1\ddot{Y}_1 = 0,\\
&\varepsilon\alpha_2\ddot{Y}_2 = 0, \forall |X - Y_1| < 1 \text{ and } |X - Y_2| < \Delta
\end{aligned} \tag{4}$$

In the same way, after substitution of Eq.(3) in Eq.(2), it becomes:

$$\begin{aligned}
&\forall |X - Y_1| = 1 \quad \text{or } |X - Y_2| = \Delta\\
&X_+ = X_-, \quad Y_{1+} = Y_{1-}, \quad Y_{2+} = Y_{2-}\\
&M\dot{X}_+ + \varepsilon\alpha_1\dot{Y}_{1+} + \varepsilon\alpha_2\dot{Y}_{2+} = M\dot{X}_- + \varepsilon\alpha_1\dot{Y}_{1-} + \varepsilon\alpha_2\dot{Y}_{2-}\\
&\text{if } |X - Y_1| = 1 \quad \dot{X}_+ - \dot{Y}_{1+} = -R\left(\dot{X}_- - \dot{Y}_{1-}\right), \quad \dot{Y}_{2+} = \dot{Y}_{2-}\\
&\text{ifi } |X - Y_2| = \Delta \quad \dot{X}_+ - \dot{Y}_{2+} = -R\left(\dot{X}_- - \dot{Y}_{2-}\right), \quad \dot{Y}_{1+} = \dot{Y}_{1-}
\end{aligned} \tag{5}$$

The barycentric coordinates are introduced in the following way:

$$V = X + \varepsilon\alpha_1 Y_1 + \varepsilon\alpha_2 Y_2, \quad W_1 = X - Y_1, \quad W_2 = X - Y_2 \tag{6}$$

These coordinates correspond to the physical displacement of the center of mass and the relative displacement of VI NES. The substitution of Eq.(6) in Eq.(4) and Eq.(5) gives:

$$
\begin{aligned}
&\ddot{V}+\frac{V+\varepsilon\alpha_1 W_1+\varepsilon\alpha_2 W_2}{1+\varepsilon}+\varepsilon\lambda\frac{\dot{V}+\varepsilon\alpha_1\dot{W}_1+\varepsilon\alpha_2\dot{W}_2}{1+\varepsilon}\\
&=\varepsilon G\sin\tilde{\Omega}T\\
&\ddot{W}_1+\frac{V+\varepsilon\alpha_1 W_1+\varepsilon\alpha_2 W_2}{1+\varepsilon}+\varepsilon\lambda\frac{\dot{V}+\varepsilon\alpha_1\dot{W}_1+\varepsilon\alpha_2\dot{W}_2}{1+\varepsilon}\\
&=\varepsilon G\sin\tilde{\Omega}T\\
&\ddot{W}_2+\frac{V+\varepsilon\alpha_1 W_1+\varepsilon\alpha_2 W_2}{1+\varepsilon}+\varepsilon\lambda\frac{\dot{V}+\varepsilon\alpha_1\dot{W}_1+\varepsilon\alpha_2\dot{W}_2}{1+\varepsilon}\\
&=\varepsilon G\sin\tilde{\Omega}T\\
&\forall|W_1|<1 \text{ and } |W_2|<\Delta
\end{aligned}
\tag{7}
$$

$$
\begin{aligned}
&\forall|W_1|=1 \quad \text{or } |W_2|=\Delta\\
&V_+=V_-, \quad W_{1+}=W_{1-},\\
&W_{2+}=W_{2-}, \quad \dot{V}_+=\dot{V}_-\\
&\text{if } |W_1|=1\\
&\dot{W}_{1+}=-R\dot{W}_{1-}, \quad \dot{W}_{2+}=\dot{W}_{2-}-\frac{\varepsilon\alpha_1(1+R)}{1+\varepsilon\alpha_1}\dot{W}_{1-}\\
&\text{if } |W_2|=\Delta\\
&\dot{W}_{2+}=-R\dot{W}_{2-}, \quad \dot{W}_{1+}=\dot{W}_{1-}-\frac{\varepsilon\alpha_2(1+R)}{1+\varepsilon\alpha_2}\dot{W}_{2-}
\end{aligned}
\tag{8}
$$

Eqs.(7) and (8) are analyzed with the multiple scales method. Solutions are found in the following form:

$$
\begin{aligned}
V(T_0,T_1)&=V_0(T_0,T_1)+\varepsilon V_1(T_0,T_1)+\ldots\\
W_1(T_0,T_1)&=W_{10}(T_0,T_1)+\varepsilon W_{11}(T_0,T_1)+\ldots\\
W_2(T_0,T_1)&=W_{20}(T_0,T_1)+\varepsilon W_{21}(T_0,T_1)+\ldots
\end{aligned}
\tag{9}
$$

with $T_i=\varepsilon^i T$. After substitution of Eq.(9) in Eq.(7) and Eq.(8), they become as follows:

- Ordre ε^0

$$\begin{aligned}
&\forall |W_{10}| < 1 \text{and } |W_{20}| < \Delta \\
&D_0^2 V_0 + V_0 = 0, \\
&D_0^2 W_{10} + V_0 = 0, \quad D_0^2 W_{20} + V_0 = 0 \\
&\forall |W_{10}| < 1 \text{or } |W_{20}| < \Delta \\
&V_{0+} = V_{0-}, \quad W_{10+} = W_{10-}, \\
&W_{20+} = W_{20-}, \quad D_0 V_{0+} = D_0 V_{0-} \\
&\text{if } |W_{10}| = 1 \\
&D_0 W_{10+} = -R D_0 W_{10-}, \quad D_0 W_{20+} = D_0 W_{20-} \\
&\text{if } |W_{20}| = \Delta \\
&D_0 W_{20+} = -R D_0 W_{20-}, \quad D_0 W_{10+} = D_0 W_{10-}
\end{aligned} \tag{10}$$

- Ordre ε^1

$$\begin{aligned}
&D_0^2 V_1 + V_1 = -\alpha_1 W_{10} - \alpha_2 W_{20} \\
&+V_0 - 2D_0 D_1 V_0 - \lambda D_0 V_0 + G \sin \Omega T_0
\end{aligned} \tag{11}$$

The solution of the first equation of Eq.(10) can be written in the following way:

$$V_0(T_0, T_1) = A(T_1) \sin\left(T_0 + \alpha(T_1)\right) \tag{12}$$

The second and third equation of Eq.(10) represent an oscillator with vibro-impacts under periodic excitations. Like in [29], Their solutions can be expressed with standard trigonometric functions as follows:

$$\begin{aligned}
&W_{j0}(T_0, T_1) = A(T_1) \sin(T_0 + \alpha(T_1)) \\
&+\tfrac{2B_j}{\pi} \arcsin(\cos(T_0 + \eta_j(T_1))), \quad j = 1, 2
\end{aligned} \tag{13}$$

Combined with the conditions of impacts given in Eq.(10), the following relations are obtained:

$$\begin{aligned} \sin(\alpha-\eta_1) &= \frac{1-B_1}{A}, \quad \cos(\alpha-\eta_1) = \frac{2B_1\delta}{A\pi} \\ \sin(\alpha-\eta_2) &= \frac{\Delta-B_2}{A}, \quad \cos(\alpha-\eta_2) = \frac{2B_2\delta}{A\pi} \end{aligned} \tag{14}$$

with $\delta = (1-R)/(1+R)$, these relations can be combined through using the trigonometric identity:

$$A^2 = (1-B_1)^2 + \frac{4B_1^2\delta^2}{\pi^2} = (\Delta-B_2)^2 + \frac{4B_2^2\delta^2}{\pi^2} \tag{15}$$

Eq.(15) represents one algebraic relation related to the displacement amplitude of LO and that of two VI NES, which is termed as SIM. In the first approximation order, the amplitude of every VI NES only depends on the amplitude of the main system and the performance of two VI NES is decoupled. It establishes the analytical foundation of the principle of separate activation as stated in [42, 43] for the case of cubic NES, which is also applicable for VI NES here.

Eq.(11) in the order ε^1 is now studied. To identify secular terms, the solutions of W_{j0} are developed in series of Fourier. The development for one harmonic gives:

$$W_{j0} = A\sin(T_0+\alpha) + \frac{8B_j}{\pi^2}\cos(T_0+\eta_j), \quad j = 1,2 \tag{16}$$

The system is studied in the vicinity of the resonance frequency of the main system. The pulsation of excitation is expressed in the following way:

$$\tilde{\Omega} = 1 + \varepsilon\sigma \tag{17}$$

After the substitution of Eqs.(12, 16) and Eq.(17) in Eq.(11), it comes:

$$\begin{aligned} & D_0^2 V_1 + V_1 \\ & = -\sum_{j=1}^{2} \left[\alpha_j \left(A \sin(T_0 + \alpha) + \frac{8B_j}{\pi^2} \cos(T_0 + \eta_j) \right) \right] \\ & -2D_1 A \cos(T_0 + \alpha) + A \sin(T_0 + \alpha)(1 + 2D_1 \alpha) \\ & -\lambda A \cos(T_0 + \alpha) + G \sin(T_0 + \sigma T_1) \end{aligned} \tag{18}$$

After arrangement, the condition for the elimination of secular term is as follows:

$$\begin{aligned} 2D_1 A &= -\sum_{j=1}^{2} \left[\frac{8\alpha_j B_j}{\pi^2} \cos(\alpha - \eta_j) \right] - \lambda A + G \sin(T_1 \sigma - \alpha) \\ 2AD_1 \alpha &= \sum_{j=1}^{2} \left[\frac{8\alpha_j B_j}{\pi^2} \sin(\alpha - \eta_j) \right] - G \cos(T_1 \sigma - T_1) \end{aligned} \tag{19}$$

The expressions of $\sin(\alpha - \eta_j)$ and $\cos(\alpha - \eta_j)$ $(j = 1, 2)$ given in Eq.(14) are substituted in Eq.(19), then the change of variable $T_1 \sigma - \alpha = \theta$ is introduced:

$$\begin{aligned} 2D_1 A &= \frac{16\alpha_1 B_1^2 \delta}{\pi^3 A} - \frac{16\alpha_2 B_2^2 \delta}{\pi^3 A} - \lambda A + G \sin\theta \\ 2AD_1 \theta &= -\frac{8\alpha_1 B_1 (1 - B_1)}{A\pi^2} - \frac{8\alpha_2 B_2 (\Delta - B_2)}{A\pi^2} + G \cos\theta + 2A\sigma \end{aligned} \tag{20}$$

The fixed points to the limit $T_1 \to \infty$ are calculated by eliminating the derivation in Eq.(20). The obtained equations can be combined by using the trigonometric identity. After rearrangement, one equation of the following form is obtained:

$$c_2 A^4 + c_1(B_1, B_2) A^2 + c_0(B_1, B_2) = 0 \tag{21}$$

Eq.(21) can be expressed in the function of only A and B_1 or B_2 by using Eq.(15). The obtained equation can be resolved for A^2.

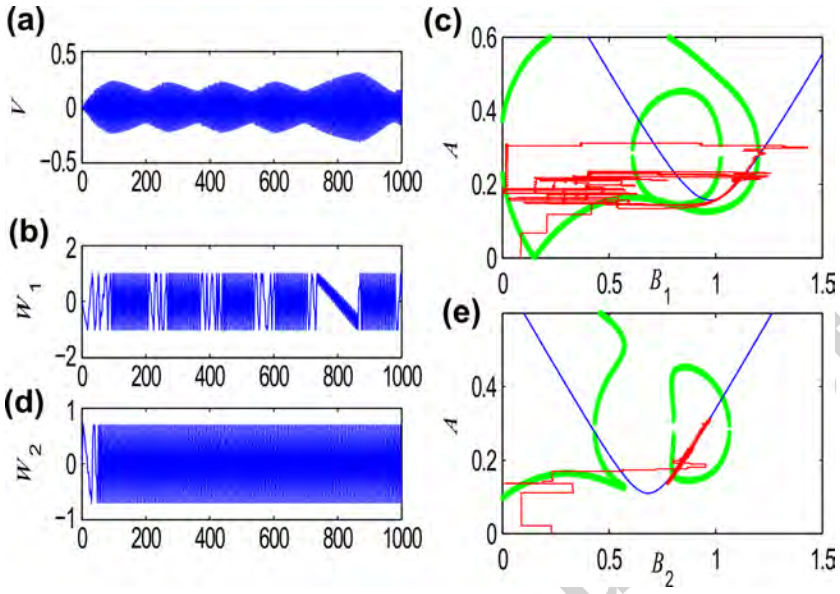

Fig. 2. Numerical integration of Eqs. (7, 8) for $G = 0.8$ and $\sigma = 0.5$: (a) SMR of V; (b) intermittent resonance of W_1 related to the first VI NES; (c) the analytically obtained SIM of the first order in blue curve and of the second order in green curve, the projection of motion for the first VI NES in red curve; (d) the constant response of W_2 related to the second VI NES; (e) the projection of motion for the second VI NES in red curve.

The thereby obtained algebraic relation between A and B_1 or B_2 represents the invariant manifold of the problem in the time-scale T_1. Subsequently, different results of numerical integration and their projections into the invariant manifold of each VI NES are presented.

3. Numerical results

In this part, the objective is to validate the analytical results by numerical simulations. The Eqs.(7) and (8) will be used. The used parameters are showed as follows:

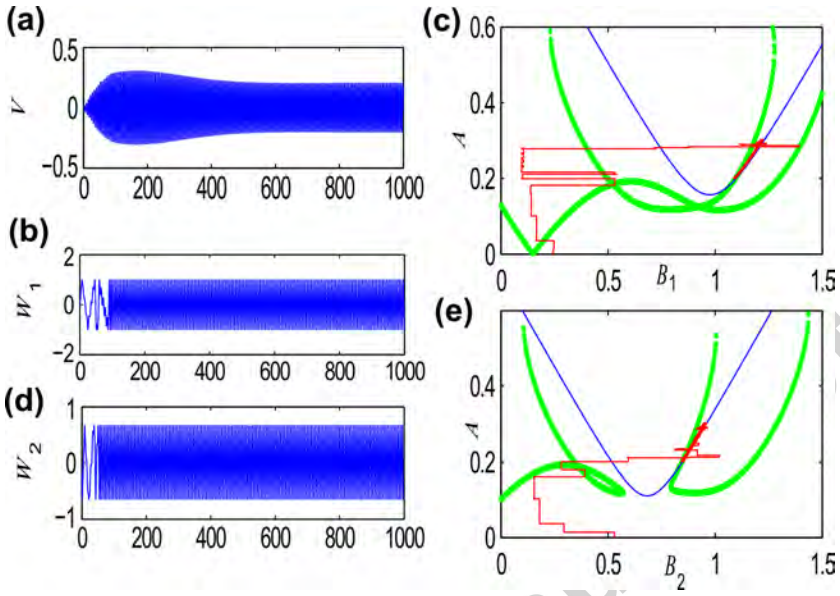

Fig. 3. Numerical integration of Eqs. (7, 8) for $G = 0.9$ and $\sigma = -0.2$: (a) steady state response of V; (b) constant resonance of W_1 related to the first VI NES; (c) the analytically obtained SIM of the first order in blue curve and of the second order in green curve, the projection of motion for the first VI NES in red curve; (d) the constant response of W_2 related to the second VI NES; (e) the projection of motion for the second VI NES in red curve.

$$\begin{aligned} &\varepsilon = 0.01, \quad \Delta = 0.7, \quad R = 0.6, \\ &\alpha_1 = \alpha_2 = 0.5, \quad \lambda = 1 \end{aligned} \tag{22}$$

The numerical integration results with SIM for $G = 0.8$ and $\sigma = 0.5$ are presented in Fig. 2. In this case, the time history of V, which is an approximate description of the displacement of LO, illustrates its strongly modulated feature [31, 34] as displayed in Fig. 2(a). Its amplitude is chaotic strongly modulated and the relative maximal amplitude is not constant every time. In Fig. 2(b), the relative displacement related to VI NES 1 is showed. The dense parts denote that

it realizes two impacts per cycle, and the sparse parts denote the occasional out of activation. Therefore, VI NES1 realizes intermittent response . Then, its response is projected to the SIM in red curve as showed in Fig. 2(c). The intersections of the blue curve and the green curve denote the fixed points, but their stabilities are not calculated here. The overlapping parts between the blue curve and the red curve demonstrate the parts with two impacts per cycle and validate the prediction accuracy of SIM. For VI NES 2, it is activated in permanence with two impacts per cycle as showed by W_2 in Fig. 2(d). Its motion is projected to SIM as showed in Fig. 2(e), and the projected A and B_2 are always in right branch of SIM. It means that the displacement amplitude of VI NES 2 will always vary simultaneously with that of LO.

Another case is presented in Fig. 3 for $G = 0.9$ and $\sigma = -0.2$. In this case, the two VI NES are attracted by fixed points, namely the intersections between the blue curve and red curve, as showed in Fig. 3 (c) and (e). The main system performs steady oscillation as displayed in Fig. 3 (a). Compared to the last case, the values of A, B_1 and B_2 are constant and well predicted by the SIMs.

Actually, the ability of SIM obtained by analytical study is limited on predicting the resonance responses with two impacts per cycle of main system or other response regimes with resonant parts. Other more complicated phenomena will be demonstrated by the following experimental study.

4. Experimental results

In this section, experiments are done for periodic and transient excitation respectively to compare the case with one VI NES and that with two VI NES. For periodic excitation, the experimentally obtained and used parameters are displayed

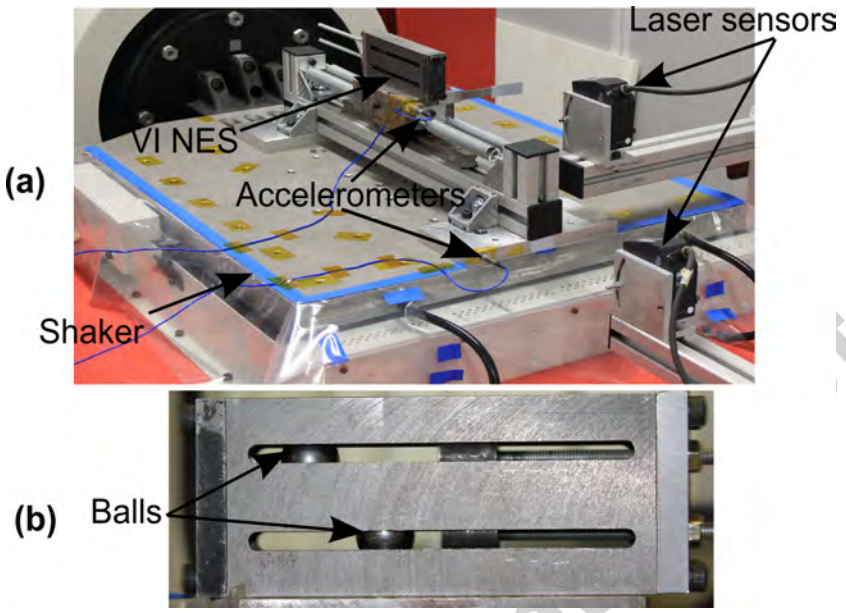

Fig. 4. Experimental setup: (a) global configuration; (b) detailed view of VI NES.

at the first place. Then, the results under excitation with a single frequency and a range of frequency around resonance frequency are demonstrated to show the possible response regimes, and to compare the efficiency under different combinations of length of cavity. Regarding transient excitation, the same experimental device is applied and the objective is to verify the principle of separate activation.

4.1. Periodic excitation

4.1.1. Experimental setup

The global experimental configuration is showed in Fig. 4(a). Two VI NES are put inside two clearances of LO in parallel as demonstrated in Fig. 4 (b), and they can move freely inside. The whole system is embedded on an electrodynamic shaker with a maximal force 10 kN. The displacement of LO as well as the im-

Table 1. Experimental parameters

Physical Parameters			
M	4.7 kg	C	3.02 Ns/m
K	$11.47 \cdot 10^3$ N/m		
m_1	32 g	m_2	32 g
b_1	$0-50$ mm	b_2	$0-50$ mm
Reduced Parameters			
ε	0.76 %	λ_1	1.91
f_0	7.86 Hz		
Single frequency test			
f_r		$7.82-7.84$ Hz	
Shaker acceleration		0.06 g	
Frequency band test			
$f_s - f_e$		$6.5-9$ Hz	
Shaker acceleration		0.06 g	

posed displacement of the shaker are measured by contact-less laser displacement sensors. Their accelerations are measured by accelerometers and the impacts between VI NES and LO can be judged from the sudden changes of the acceleration of LO. A detailed view of the configuration for two VI NES is presented in Fig. 4 (b). It simply consists of two closed clearances of lengths $d+2\cdot b1$ and $d+2\cdot b2$, respectively, where d is the diameter of both balls (VI NES). $b1$ and $b2$ are lengths of the above clearance and the below clearance, respectively, and each can be adjusted by a cylinder. The cylinder and the cover at the opposite side are made of hardened steel. The parameters of this system have been identified by performing modal analysis and are summarized in Table 1.

4.1.2. Single frequency excitation

The frequency of the sinusoidal excitation is slowly varied from 7.82 Hz to 7.84 Hz during 80 s, which can be considered almost fixed to the value 7.83 Hz. This value is closed to the natural frequency of LO ($f_0 = 7.86$ Hz). The acceleration of the shaker is fixed to 0.06 g. During the whole experimental process, the time histories of displacement and acceleration of LO are recorded.

With the change of the number of VI NES and different combinations of clearances b1 and b2, different periodic and transient response regimes are observed and demonstrated here. They are identified by the difference of impact numbers per cycle of LO, which can be judged from the time history of the acceleration of LO.

At first, the time history of the acceleration of LO without VI NES is showed in Fig. 5(a) as a reference. Although there exist small shakes at some of its maximal place, no impacts exist. In addition, its amplitude is highest compared to other cases coupled with VI NES. Then, the time history of the acceleration of LO with

a VI NES for a clearance of 30 mm is showed in Fig. 5(b) as another reference. This value of clearance is proved to be almost optimal in the sense of vibration control and the response regime is two impacts per cycle [36]. It is not so easy to distinguish impacts because the order of impact strength is close to that of the acceleration of LO, but the impact number is observable during the process of experiment. Moreover, the peaks of acceleration are evidently reduced compared to the results in Fig. 5(a).

With the addition of another ball and different combinations of clearances, the response regimes will be more complicated. However, the possible variations are always based on the above two cases. Then, the regime with four impacts per cycle is observed with the addition of a second ball with clearance $b1 = 5$ mm (another ball with clearance $b2 = 30$ mm), and both ball impact twice per cycle as showed in Fig. 5(c), and the four impact moments during one cycle are marked out in rectangles. The acceleration of LO is further decreased compared to the optimized one ball case with 30 mm clearance, and this efficiency improvement cannot be easily judged here and will be demonstrated from the viewpoint of displacement later.

When the clearance of the added ball is increased to 40 mm, the response is complicated as displayed in Fig. 5(d). The ball below with $b2 = 30$ mm continuously impacts twice per cycle. In contrast, the added ball impacts only once during many cycles (> 1), and a few of them are marked out in rectangles.

In addition to the above relative stable response regimes, there exist some even more complicated transient response regimes during one time history for some combinations of clearances. For the case with $b1 = b2 = 30$ mm, there are some periods as showed in Fig. 5(e), in which just one ball is activated with two

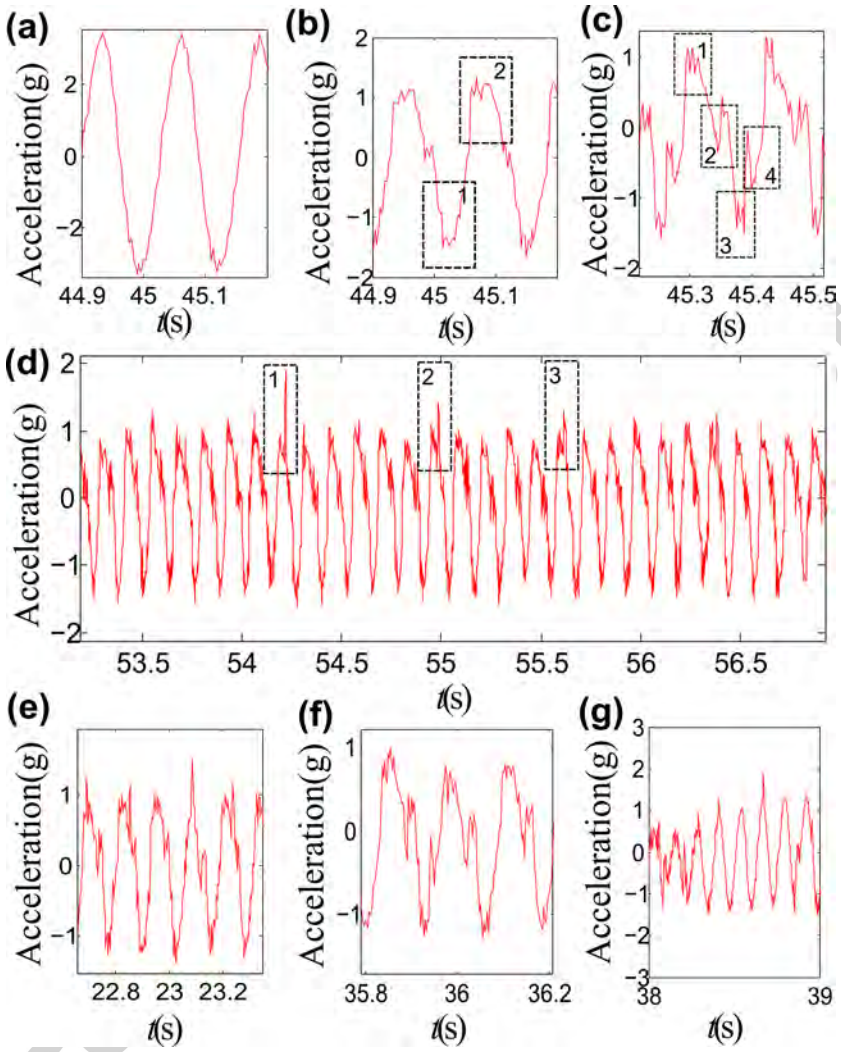

Fig. 5. Typical response regimes by comparison of impact numbers per cycle of the acceleration of LO and some impacts moments are marked out in rectangle: (a) no impact and no VI NES; (b) two impacts per cycle; (c) four impacts per cycle; (d) one VI NES impacts once during many cycles and another VI NES impacts twice per cycle; (e) one period of a response with at least one VI NES in the state of two impacts per cycle; (f) one period of a response with both VI NES in the state of two impacts per cycle; (g) one period of a response with both VI NES out of activation and no impact.

impacts per cycle, but this activated state can alternate between these two balls. This phenomenon is complicated, and it cannot be judged from the results showed here and can just be observed in the test site. There are also some periods, two balls impact twice per cycle as showed in Fig. 5(f) and there are even some periods there are almost no impacts as showed in Fig. 5(g).

Therefore, the strong nonlinear coupling between these two balls and LO is well observed by the complicated variations of response regimes during one time history. The above mentioned basic response regimes will be applied to explain the complication variation of efficiency, and this point is closely related to the targeted energy transfer by transient resonance captures.

In [36], it is observed that the optimal response regime is the one with two impacts per cycle and around the entrance of SMR. The idea of optimization design is to make efficient response regimes occur for different excitations. This idea can still apply in the optimization design of two VI NES, namely to make each VI NES activated at its best state with two impacts per cycle.

Then, the efficiency comparison of different combinations of clearances is performed here to observe the possible relation between the types of response regimes and their efficiency. The two cases without VI NES and with one optimized VI NES (30 mm clearance) are chosen as two references as showed in Fig. 6(a-b).

The length of the down clearance $b2$ is fixed to 30 mm and only the upper clearance $b1$ is varied from 5 mm to 50 mm. Here, only the time histories of displacement are demonstrated for $b1 = 30$ mm and $b1 = 5$ mm, respectively. The former is displayed in Fig. 6(a), there are three typical areas A1, A2 and A3, which correspond to typical response regimes from Fig. 5(e) to Fig. 5(g), respectively. In area A1, there is a small decrease of amplitude compared to the

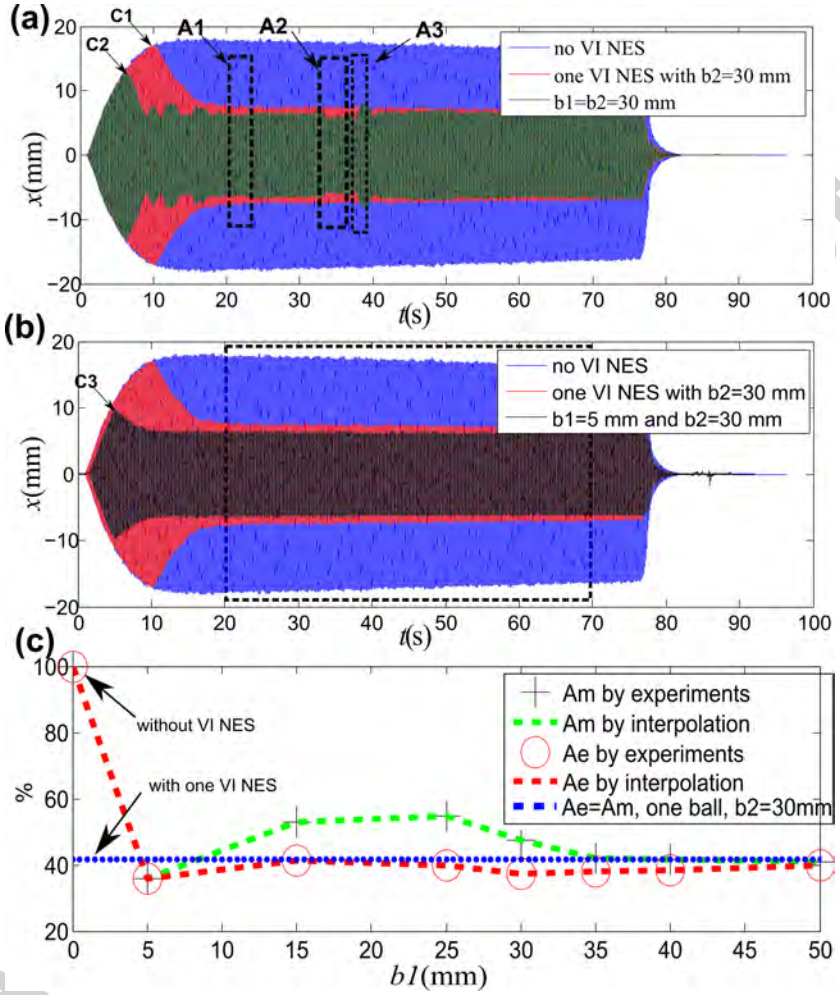

Fig. 6. Typical response regimes and their efficiency comparison with different combinations of clearances: (a-b) response regimes; (c) efficiency comparison by average and maximal amplitude ratios (Ae and Am).

one VI NES case in red curve. In area A2, both ball impact twice per cycle and the amplitude is lowest. In area A3, the occasional out of activation for both balls and the amplitude increases. In the whole process, there are many transitions between them, which results in the complicated variation of displacement amplitude of LO. It is a direct proof of nonlinear coupling between two VI NES and LO. In addition, the efficiency is highest when both balls impact twice per cycle, which is the most effective form of transient resonance captures.

This efficient targeted energy transfer is better demonstrated by the decrease of b1 to 5 mm as showed in Fig. 6(b). This time, both VI NES impact twice per cycle and it means the permanent resonance captures.

With the excitation of LO at the beginning, different activation amplitudes of LO with different combinations of clearances are observed, namely C1, C2 and C3 in Fig. 6(a-b). With the increase of VI NES from 0 to 1, and then 2, the amplitude is evidently decreased at the activation point of VI NES. The same conclusion is obtained when the value of another clearance is decreased. In this sense, the robustness and efficiency can be improved.

Then, the average and maximal amplitude ratios between the case with VI NES and without NES are calculated for all cases during a stable time period (20-70 s), and the results are showed in Fig. 6(c). Compared to the case without VI NES and with one VI NES, the optimal case is the addition of another VI NES with a small clearance 5 mm. For other cases with large clearances, it cannot improve the efficiency and, in return, it will result in the occasional out of activation of VI NES, and meanwhile, the large displacement of LO.

According to the optimization design criterion proposed in [36], the design of parameters is to make the efficient response regimes appear and it means the

most efficient transfer and dissipation of energy. From the above experimental results with limited combinations of clearances, this optimization design criterion still applies since both balls impacts twice in the optimal case with $b1 = 5$ mm. However, the phase difference of two VI NES cannot be measured or calculated, it may be another factor related to efficiency.

Except the above combinations of clearances, experiments with the same clearance for both VI NES are also performed. The average and maximal amplitude ratios are also calculated and showed in Fig. 7. From the viewpoint of Ae, the case with $b1 = b2 = 30$ mm is optimal. On the contrary, the case with $b1 = b2 = 15$ mm is optimal in terms of Am. Generally speaking, they are less effective than the combination with $b1 = 5$ mm and b2=30 mm.

As a summary, the objective to find the relation between response regimes and their efficiency is accomplished in two steps. The first step is to find basic response regimes. Then, they are applied to explain the complicated variation of response. As a result, a general design criterion can also be proposed here: the design of two VI NES is to make them activated around most efficient response regimes.

4.1.3. Excitation with a band of frequency

Then, the band of excitation frequency is enlarged around the natural frequency of LO. The objective here is to study the influence of different combinations of clearances on the response regimes and their efficiency. The starting frequency f_s and ending frequency f_e during this sweep is showed in Table 1 and the acceleration is still fixed to 0.06 g.

For the above experimental configuration, the one VI NES case with a clearance 27.5 mm has been observed optimal [36]. Here the clearance of an added

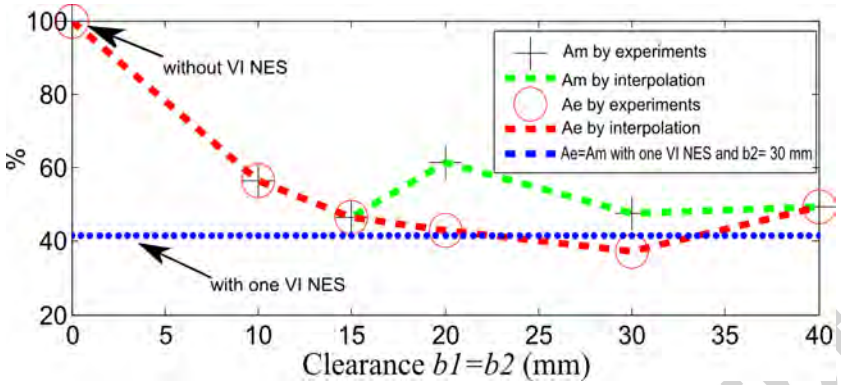

Fig. 7. Efficiency comparison of different response regimes with the same clearance for both VI NES.

VI NES is selected around this value. The displacement of LO is recorded for different combinations of $b1$ and $b2$ and is showed in Fig. 8. The results with fixed $b2 = 27.5$ mm and varying $b1$ are showed in Fig. 8(a). The combination of $b1 = 12.5$ mm and $b2 = 27.5$ mm is generally more optimal in this case. Then, the results with equal $b1$ and $b2$ are showed in Fig. 8(b). For frequencies a little below the resonance frequency, the combination of $b1 = 27.5$ mm and $b2 = 27.5$ mm is better, but the other two are better for frequencies a little higher than the resonance frequency. To have a close view, the results between two relative optimal cases are compared in Fig. 8(c). In area A, it is observed that VI NES can be activated at a lower value of displacement amplitude for a smaller $b1$. In area B, two VI NES are in regime with two impacts per cycle for $b1 = 27.5$ mm. On the contrary, one ball occasionally gets out of activation for $b1 = 12.5$ mm and results in the transient build-up of amplitude. In area C, low $b1 = 12.5$ mm still can be activated for lower amplitude and results in the reduction of amplitude. As has been demonstrated under the excitation with a fixed frequency, the variation

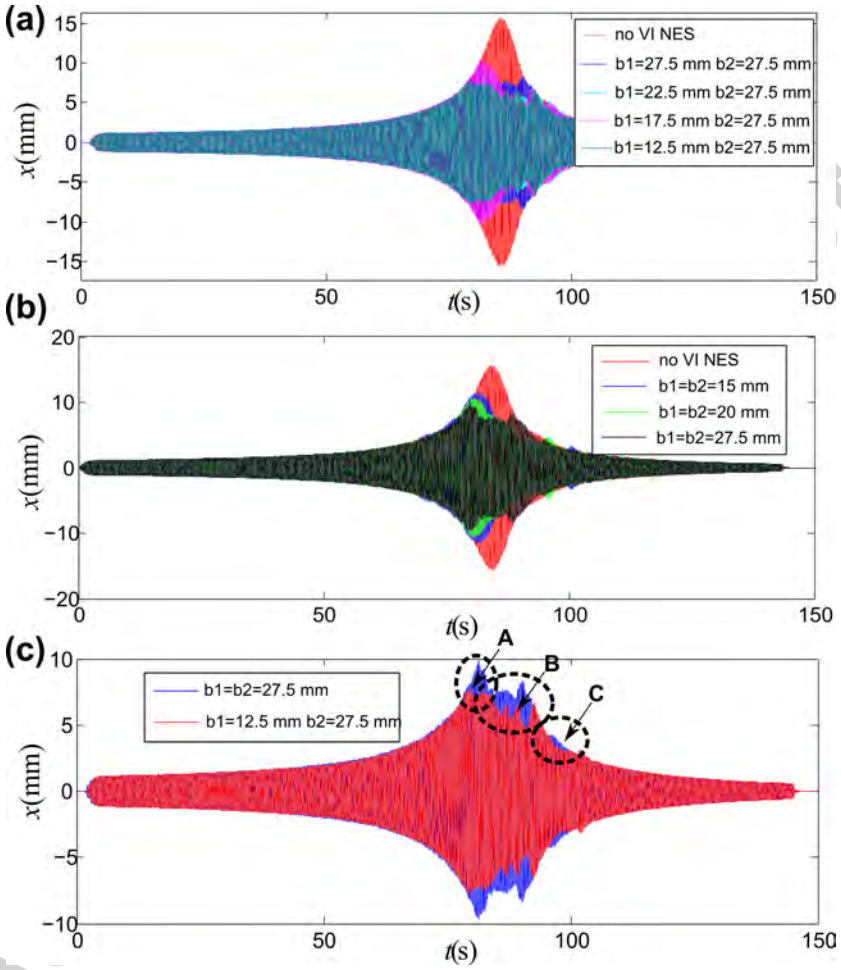

Fig. 8. Responses of LO during the sweep experiments and efficiency comparison: (a) with different $b1$ and $b2$; (b) with the same $b1$ and $b2$; (c) the efficiency comparison for two relative optimal cases.

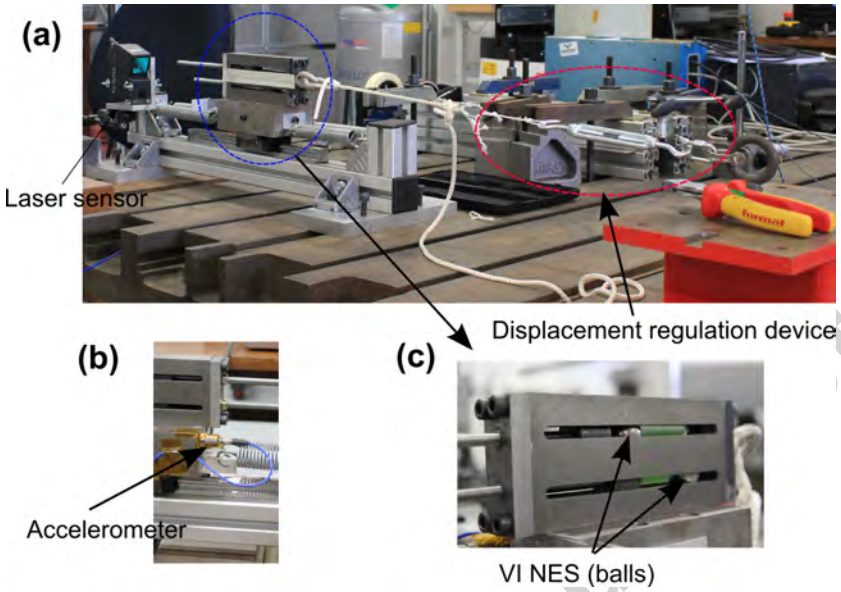

Fig. 9. Experimental setup: (a) global configuration; (b) installation of accelerometer; (c) detailed view of VI NES.

of motion for LO and both VI NES can be more complicated than the above-mentioned characteristics. Except the observed relation between efficiency and the response regimes, it is desirable to obtain further information but this kind of try would be difficult.

Therefore, the following optimization design criterion is recommended. If just one ball is applied, it is recommended that VI NES should be optimized at the point of natural frequency. If two VI NES are applied to improve the robustness and increase efficiency, a smaller length of clearance should be chosen compared to the optimized clearance of the one ball case to avoid the occasional failure.

4.2. Transient excitation

4.2.1. Experimental setup

The same experimental device as the periodic case is used, but it is attached to a cast iron bench as showed in Fig. 9(a). The addition of a small ring bolt for pre-stretch will not influence the total mass of LO and its influence can be neglected. Therefore, its parameters are nearly the same as these in Table 1. One laser sensor and one accelerometer are used to measure the displacement and acceleration of LO, respectively. The fixation of accelerometer is showed in Fig. 9(b) and a detailed view of VI NES is displayed in Fig. 9(c). The number of balls can be changed. The initial displacement of LO is regulated by a device and is fixed to 20 mm for all tests. The initial location of two balls are at random, and the velocities for LO and both balls are zero. Since only the stable transition process is studied and the transient process quickly disappears, the initial conditions will not influence the expected conclusion.

4.2.2. Principle of separate activation

With two sets of $b1$ and $b2$, the responses of two cases are compared here. For the case with one VI NES ($b2 = 20$ mm), the time history of displacement of LO is represented by the red curve in Fig. 10(a) and its corresponding acceleration is showed in Fig. 10(b). The points A1 and A2 are related to the transition from the regime with two impacts per cycle to that without any continuous period of two impacts per cycle.

For the case with two balls ($b1 = 2$ mm and $b2 = 20$ mm), the time history of displacement of LO is represented by the blue curve in Fig. 10(a) and its corresponding acceleration is showed in Fig. 10(c). The first VI NES with $b2 = 20$ mm gets out of two impacts per cycle around points B1 and B2. The second VI

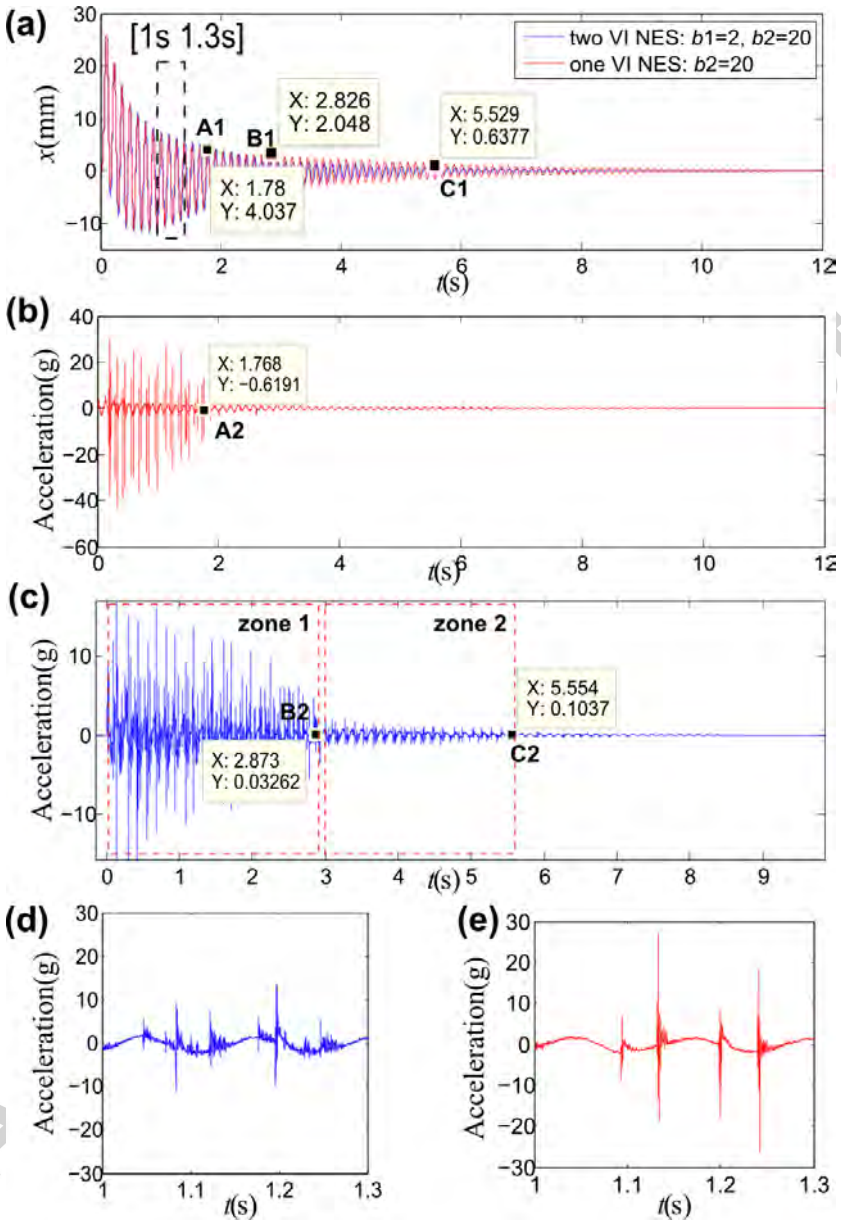

Fig. 10. Response comparison between LO coupled with one VI NES and two VI NES: (a) an imposed time history of displacement; (b) a time history of acceleration with one VI NES; (c) a time history of acceleration with two VI NES; (d) a detailed view of one period of acceleration with two VI NES; (e) a detailed view of one period of acceleration with one VI NES.

NES with a small clearance $b1 = 2$ mm gets out of two impacts per cycle around points C1 and C2. In zone 1, the first VI NES with a large clearance is activated with two impacts per cycle. In zone 2, the first VI NES gets out of activation and the second VI NES with a small clearance is activated with two impacts per cycle. In the sense of the activation with two impacts per cycle, the principle of separate activation of VI NES with different clearances is observed here. This definition of activation is important, since the regime with two impacts per cycle is most efficient in vibration control [36].

Then, the decay rates of displacements for both cases are compared. Before point A1, there is almost no difference, since the first VI NES with large clearance is activated with two impacts per cycle and the second VI NES behaves in low efficient regime (more than two impacts per cycle). Between A1 and B1, the role of the second VI NES increases but still small. In contrast, it plays an important role between B1 and C1 since it is activated with two impacts per cycle and the first VI NES is totally out of excitation. The difference of decay rates in this period is relative large. Here, the role of separate activation in vibration control is evident, and the two VI NES with difference clearances can be effective at different ranges of displacement amplitude. More importantly, this effectiveness is related to the efficient response regime with two impacts per cycle.

During the above transition process, the first VI NES changes from two impacts per cycle to the state with no continuous periods of two impacts per cycle (i.e., permanent out of activation), the limit point is A1. It means that it plays the main role in vibration control before A1. In contrast, the second VI NES changes from more than two impacts per cycle to two impacts per cycle, and finally out of activation, it plays a main role in vibration control between B1 and C1. Between

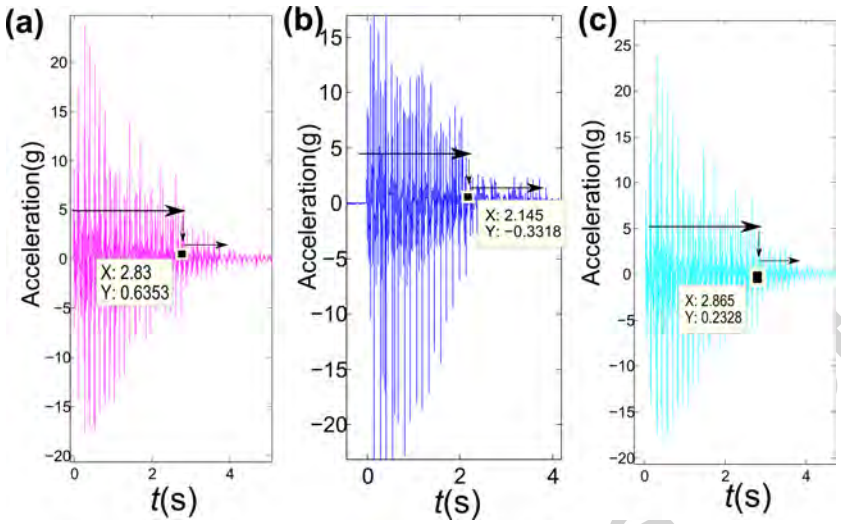

Fig. 11. Principle of separate activation: (a) $b1 = 5$ mm and $b2 = 20$ mm; (b) $b1 = 5$ mm and $b2 = 30$ mm; (c) $b1 = 5$ mm and $b2 = 40$ mm.

A1 and B1, it is the overlapping period. Evidently, the second VI NES undergoes more response regimes and could possess four impacts per cycle, three impacts per cycle and two impacts per cycle etc., which are closely related to different transient resonance captures.

In addition to displacement decay rates, impacts reflected by acceleration can also reveal some important characteristics. The time histories of acceleration of LO from 1 s to 1.3 s are taken out for both cases, as showed in Fig. 10(d) for two VI NES case and in Fig. 10(e) for one VI NES case. With the addition of another ball, the impact strengths are decreased and the impacts are scattered. As observed by other researchers, the regime with strong impact strengths but less impact numbers is replaced by that with weak and more impacts, but the whole energy reduction rate is not improved.

The principle of separate activation is also observed from results with other

combinations of clearances as showed in Fig. 11. The separate points for the out of activation of the VI NES with a large clearance are marked out in each subfigure. The horizontal arrows demonstrate the two activation levels for two different clearances, and the vertical arrows denote the change between them.

In summary, the principle of separate activation of VI NES is observed, and the effectiveness of the vibration control can be increased to a large range of displacement amplitude of LO. Moreover, the addition of VI NES can reduce impact strengths and scatter impacts though it may not increase the efficiency of vibration control.

5. Conclusion

A LO coupled with two VI NES in parallel is studied under periodic and transient excitations. Firstly, the system is analytically studied with the multiple scales method. SIM is obtained and fixed points can be calculated. Then, numerical simulations are performed to observe the typical response regimes and to validate the analytical results. Finally, experiments under different types of excitations are carried out to observe the possible response regimes and to compare the efficiency of different combinations of clearances.

The asymptotic method, which has been proved feasible for the analytical study of systems coupled with one VI NES, is generalized to the case with two VI NES. Two different SIMs are obtained for two VI NES with different clearances. Since a SIM is related to an activation threshold, namely displacement amplitude of LO, the analytically obtained two different SIMs can explain the principle of separate activation. This principle can be more directly reflected by the transient excitation case. In addition to SIM, fixed points can be calculated and their po-

sition can be applied to judge the types of response regimes. Compared to the former analytical methods, the variation of transient and modulated response can be further explained this time. Numerical results prove the consistency of analytical prediction of two classic response regimes, namely two impacts per cycle and SMR. More specifically about SMR, its existence and its periods with two impacts per cycle can be well predicted by SIM.

Although analytical study is limited to obtain results for regimes with two impacts per cycle and SMR, or any combinations of these two regimes, they are still important. From the viewpoint of TET by resonance captures, these regimes possess the most efficient permanent or transient resonance captures.

Through experiments under different excitations, different response regimes are observed and their relation to their efficiency is analyzed. Whatever types of excitation, it is more effective as long as the two VI NES are activated with two impacts per cycle or around this regime. In addition to this common law, the results are complicated from the viewpoint of each excitation type. This observation proves the relevance and effectiveness of analytical study around SIM, more precisely, around the response regime with two impacts per cycle (i.e., resonance captures).

More specifically about experimental results, several points should be pointed out. Firstly , different basic periodic and transient response regimes are observed and analyzed from the experimental results under excitation with a fixed frequency. In addition, more complicated responses are observed but they can be explained by these basic response regimes. Then, they are applied to explain the complicated variation of response regimes, not only for excitation with a fixed frequency and a range frequency, but also for transient excitation. All observations

here prove the important role of the regime with two impacts per cycle. Under transient excitation, this role is further demonstrated by the separate activation of VI NES of different clearances. This separate activation of VI NES with two impacts per cycle can be applied to control vibration at different levels of displacement amplitude. Sometimes, although the addition of VI NES cannot improve the efficiency of vibration control, the impacts are scattered and their strengths are reduced.

In a word, many aspects of the dynamics are further explained by the analytical, numerical and experimental studies, but other factors, such as the friction between LO and VI NES, inclinations of clearances and impact models, should be considered in the analytical treatment to improve the accuracy of explanation.

Acknowledgments

The authors acknowledge the French Ministry of Science and the Chinese Scholarship Council [grant number: 201304490063] for their financial support.

[1] D. M. McFarland, L. A. Bergman, A. F. Vakakis, Experimental study of nonlinear energy pumping occurring at a single fast frequency, Int. J. Non-Linear Mech. 40 (6) (2005) 891–899.

[2] E. Gourc, G. Michon, S. Seguy, A. Berlioz, Experimental investigation and design optimization of targeted energy transfer under periodic forcing, J. Vib. Acoust. 136 (2) (2014) 021–021.

[3] R. Bellet, B. Cochelin, P. Herzog, P.-O. Mattei, Experimental study of targeted energy transfer from an acoustic system to a nonlinear membrane absorber, J. Sound Vib. 329 (14) (2010) 2768–2791.

[4] P.-O. Mattei, R. Ponçot, M. Pachebat, R. Côte, Nonlinear targeted energy transfer of two coupled cantilever beams coupled to a bistable light attachment, J. Sound Vib. 373 (2016) 29–51.

[5] S. Benacchio, A. Malher, J. Boisson, C. Touzé, Design of a magnetic vibration absorber with tunable stiffnesses, Nonlinear Dyn. (2016) 1–19.

[6] C.-H. Lamarque, O. V. Gendelman, A. T. Savadkoohi, E. Etcheverria, Targeted energy transfer in mechanical systems by means of non-smooth nonlinear energy sink, Acta Mech. 221 (1-2) (2011) 175–200.

[7] P. Lieber, D. Jensen, An acceleration damper: development, design and some applications, Trans. ASME 67 (10) (1945) 523–530.

[8] R. A. Ibrahim, Vibro-impact dynamics: modeling, mapping and applications, Vol. 43, Springer Science & Business Media, 2009.

[9] V. I. Babitsky, Theory of vibro-impact systems and applications, Springer Science & Business Media, 2013.

[10] S. Masri, T. Caughey, On the stability of the impact damper, J. Appl. Mech. 33 (3) (1966) 586–592.

[11] C. Bapat, N. Popplewell, K. McLachlan, Stable periodic motions of an impact-pair, J.Sound Vib. 87 (1) (1983) 19–40.

[12] N. Popplewell, C. Bapat, K. McLachlan, Stable periodic vibroimpacts of an oscillator, J. Sound Vib. 87 (1) (1983) 41–59.

[13] C. Bapat, S. Sankar, Single unit impact damper in free and forced vibration, J. Sound Vib. 99 (1) (1985) 85–94.

[14] F. Peterka, More detail view on the dynamics of the impact damper, Mechanics, Automatic Control and Robotics 3 (14) (2003) 907–920.

[15] S. Masri, Effectiveness of two-particle impact dampers, J. Acoust. Soc. Am 41 (6) (1967) 1553–1554.

[16] S. Masri, Analytical and experimental studies of multiple-unit impact dampers, J. Acoust. Soc. Am 45 (5) (1969) 1111–1117.

[17] C. Cempel, The multi-unit impact damper: equivalent continuous force approach, J. Sound Vib. 34 (2) (1974) 199–209.

[18] C. Bapat, S. Sankar, N. Popplewell, Experimental investigation of controlling vibrations using multi-unit impact damper, Shock Vib Bull 4 (1983) 1–12.

[19] N. Popplewell, Y. Muzyka, C. Bapat, K. McLachlan, Stable periodic motion of multiple-unit impacting mechanisms, J. Sound Vib. 86 (4) (1983) 587–593.

[20] C. Bapat, S. Sankar, Multiunit impact damper- re-examined, J. Sound Vib. 103 (4) (1985) 457–469.

[21] Y. Lee, A. F. Vakakis, L. Bergman, D. McFarland, G. Kerschen, F. Nucera, S. Tsakirtzis, P. Panagopoulos, Passive non-linear targeted energy transfer and its applications to vibration absorption: a review, P. I. Mech Eng. K-J Mul. 222 (2) (2008) 77–134.

[22] A. F. Vakakis, O. Gendelman, L. Bergman, D. McFarland, G. Kerschen,

Y. Lee, Nonlinear targeted energy transfer in mechanical and structural systems, Vol. 156, Springer Science & Business Media, 2008.

[23] F. Nucera, A. Vakakis, D. McFarland, L. Bergman, G. Kerschen, Targeted energy transfers in vibro-impact oscillators for seismic mitigation, Nonlinear Dyn. 50 (3) (2007) 651–677.

[24] F. Nucera, F. Lo Iacono, D. McFarland, L. Bergman, A. Vakakis, Application of broadband nonlinear targeted energy transfers for seismic mitigation of a shear frame: Experimental results, J. Sound Vib. 313 (1) (2008) 57–76.

[25] I. Karayannis, A. Vakakis, F. Georgiades, Vibro-impact attachments as shock absorbers, P. I. Mech. Eng. C-J Mec. 222 (10) (2008) 1899–1908.

[26] Y. Lee, F. Nucera, A. Vakakis, D. McFarland, L. Bergman, Periodic orbits, damped transitions and targeted energy transfers in oscillators with vibro-impact attachments, Physica D 238 (18) (2009) 1868–1896.

[27] O. V. Gendelman, Bifurcations of nonlinear normal modes of linear oscillator with strongly nonlinear damped attachment, Nonlinear Dynamics 37 (2) (2004) 115–128.

[28] O. Gendelman, Y. Starosvetsky, M. Feldman, Attractors of harmonically forced linear oscillator with attached nonlinear energy sink i: Description of response regimes, Nonlinear Dynamics 51 (1-2) (2008) 31–46.

[29] O. Gendelman, Analytic treatment of a system with a vibro-impact nonlinear energy sink, J. Sound Vib. 331 (21) (2012) 4599–4608.

[30] E. Gourc, G. Michon, S. Seguy, A. Berlioz, Targeted energy transfer under harmonic forcing with a vibro-impact nonlinear energy sink: Analytical and experimental developments, J. Vib. Acoust. 137 (3) (2015) 031008.

[31] O. Gendelman, A. Alloni, Dynamics of forced system with vibro-impact energy sink, J. Sound Vib. 358 (2015) 301–314.

[32] G. Pennisi, C. Stéphan, G. Michon, Vibro-impact nes: A correlation between experimental investigation and analytical description, in: Sensors and Instrumentation, Volume 5, Springer, 2016, pp. 137–142.

[33] T. Li, S. Seguy, A. Berlioz, Dynamics of cubic and vibro-impact nonlinear energy sink: Analytical, numerical, and experimental analysis, J. Vib. Acoust. 138 (3) (2016) 031–010.

[34] O. Gendelman, A. Alloni, Forced system with vibro-impact energy sink: Chaotic strongly modulated responses, Procedia IUTAM 19 (2016) 53–64.

[35] T. Li, S. Seguy, A. Berlioz, On the dynamics around targeted energy transfer for vibro-impact nonlinear energy sink, Nonlinear Dynamics (2016) 1–14doi:10.1007/s11071-016-3127-0.
URL http://dx.doi.org/10.1007/s11071-016-3127-0

[36] T. Li, S. Seguy, A. Berlioz, Optimization mechanism of targeted energy transfer with vibro-impact energy sink under periodic and transient excitation, Nonlinear Dynamics (2016) 1–19doi:10.1007/s11071-016-3200-8.
URL http://dx.doi.org/10.1007/s11071-016-3200-8

[37] E. Gourc, S. Seguy, G. Michon, A. Berlioz, B. Mann, Quenching chatter

565 instability in turning process with a vibro-impact nonlinear energy sink, J.
566 Sound Vib. 355 (2015) 392–406.

567 [38] B. Bergeot, S. Bellizzi, B. Cochelin, Analysis of steady-state response
568 regimes of a helicopter ground resonance model including a non-linear en-
569 ergy sink attachment, Int. J. Non-Linear Mech. 78 (2016) 72–89.

570 [39] F. Georgiades, A. F. Vakakis, G. Kerschen, Broadband passive targeted en-
571 ergy pumping from a linear dispersive rod to a lightweight essentially non-
572 linear end attachment, Int. J. Non-Linear Mech. 42 (5) (2007) 773–788.

573 [40] S. Tsakirtzis, G. Kerschen, P. N. Panagopoulos, A. F. Vakakis, Multi-
574 frequency nonlinear energy transfer from linear oscillators to mdof essen-
575 tially nonlinear attachments, Journal of Sound and Vibration 285 (1) (2005)
576 483–490.

577 [41] S. Tsakirtzis, P. N. Panagopoulos, G. Kerschen, O. Gendelman, A. F.
578 Vakakis, L. A. Bergman, Complex dynamics and targeted energy transfer
579 in linear oscillators coupled to multi-degree-of-freedom essentially nonlin-
580 ear attachments, Nonlinear Dynamics 48 (3) (2007) 285–318.

581 [42] B. Vaurigaud, A. T. Savadkoohi, C.-H. Lamarque, Targeted energy transfer
582 with parallel nonlinear energy sinks. part i: design theory and numerical
583 results, Nonlinear Dyn. 66 (4) (2011) 763–780.

584 [43] A. T. Savadkoohi, B. Vaurigaud, C.-H. Lamarque, S. Pernot, Targeted energy
585 transfer with parallel nonlinear energy sinks, part ii: theory and experiments,
586 Nonlinear Dyn. 67 (1) (2012) 37–46.

[44] Z. Lu, X. Lu, S. F. Masri, Studies of the performance of particle dampers under dynamic loads, J. Sound Vib. 329 (26) (2010) 5415–5433.